Energetic Ion Beam Source and Free-Stream Beam Diagnostic Techniques

R. L. Stenzel and B. H. Ripin

Department of Physics, University of California, Los Angeles, California 90024

(Received 9 November 1972; and in final form, 22 January 1973)

A steady state, dc discharge, electrostatically focused ion beam source with permanent magnet multipole confinement is described. The ion beam is low density, $n_b \sim 10^8$ cm^{-3}, low divergence, $\theta \sim 1°$, energetic, $V_b \leq 5$ kV, and is suitable for investigating ion beam–plasma interactions. Ion beam speed and species are determined either by modulating the beam and analyzing the resulting free-streaming perturbations or by a pulse and time-of-flight technique. The amplitude of the free-streaming signal is enhanced in the electron cyclotron harmonic passbands due to the decreased dielectric function of the background plasma. Two beam–plasma instabilities, the electron cyclotron drift instability, and an instability at the lower hybrid frequency are observed using this ion source.

INTRODUCTION

Several plasma instabilities have been predicted to occur when an energetic ion beam traverses a plasma perpendicular to a magnetic field.[1] Some of these instabilities have been investigated in computer simulations[2] such as the electron cyclotron drift instability, but detailed laboratory experiments are just emerging.[3] These effects may be of importance to the controlled fusion effort since the above situation occurs in magnetic pinches[4] and in neutral beam injection schemes.

We describe here a steady state, dc discharge, electrostatically focused ion beam source with multipole confinement. This source produces a low density, $n_i \simeq 10^8$ cm^{-3}, low divergence, $\theta \simeq 1^0$, energetic, $V_b \lesssim 5$ kV, ion beam suitable for investigating ion beam–plasma instabilities. The ion beam speed and species are determined by either modulating the beam ($f_m \simeq 100$ MHz, $V_m/V_b \simeq 0.01$) and analyzing the free-streaming perturbations detected by a probe downstream in an interferometer setup, or by a pulse and time-of-flight technique. It is found that H^+ H_2^+, and H_3^+ are all present in a hydrogen ion beam with the predominant species being H_2^+ or H_3^+ depending upon the neutral gas pressure in the source.

These methods are simple diagnostic techniques which avoid, for most purposes, the need for energy, velocity, and mass analyzers which can present problems due to secondary emission or ion sputtering. Analysis of the damping of the free-stream modulation on the ion beam can give information on effects which tend to phase mix the modulation such as collisions or microturbulence. In this way a noninteracting low density modulated ion beam can be used as test particles for plasma diagnostics.

It is found that the amplitude of the ion beam free-streaming perturbation is enhanced in the electron cyclotron harmonic passbands in the presence of a background plasma. This effect is interpreted to be caused by the approximate matching of the free-streaming perturbation frequency and wave number to the Bernstein wave dispersion relation where the magnitude of the plasma dielectric function decreases.

Finally, we have experimentally observed two instabilities, not previously studied, i.e., the electron cyclotron drift instability and an instability at the lower hybrid frequency.

DESCRIPTION OF THE ION BEAM SOURCE

The experimental apparatus is shown in Fig. 1. A large plasma device (1 m diam × 2 m long) contains the ion source, internally mounted Helmholtz magnetic field coils,[5] and diagnostic grids and probes. The background plasma in the large experimental chamber is produced by a dc discharge[6] and/or ionization by the ion beam of the background neutral gas ($p \lesssim 1$ mTorr). This plasma is not necessary for the operation of the ion source or its diagnostics but does provide a suitable plasma for the study of ion beam–plasma interactions.

Source

A sketch of the ion source is shown in Fig. 2. A plasma is produced in the inner chamber by ionization of the neutral

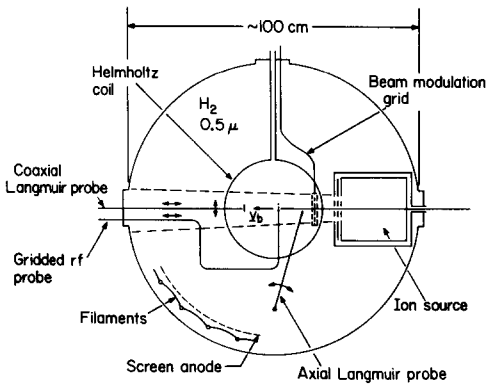

FIG. 1. Experimental arrangement of the ion source in a background plasma device with probe diagnostics.

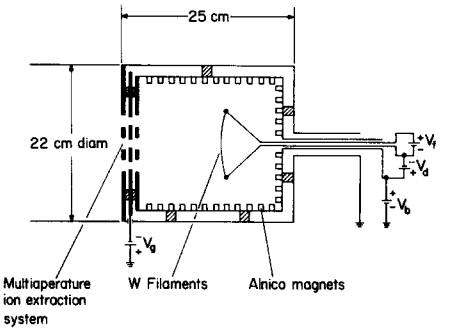

FIG. 2. Schematic of the ion source. Typical power supply data are: Filaments $V_f = 10$ V, $I_f = 30$ A; discharge $V_d = 36$ V, $I_d = 0-3$ A; beam $V_b = 0-5$ kV, $I_b = 0-400$ mA; focusing electrode grid $V_g = -50$ to -500V.

background gas by means of a dc discharge between four heated tungsten filaments biased 40 V negative with respect to the chamber walls. The quiescence of the resulting plasma is good (measured for frequencies below the ion plasma frequency) if the electron emission from the filaments is kept below 100 mA/cm. The plasma chamber interior surface is lined with permanent magnets (6.35 mm×6.35 mm×12.7 mm long Alnico V) arranged in a line cusp geometry. This multipole arrangement, first used by Limpaecher and MacKenzie,[7] improves the plasma density uniformity across the chamber, which is essential for good focusing, and efficiently increases the plasma confinement, which enables one to produce a given ion density with reduced discharge current. The extraction region is not lined with magnets so as not to perturb the ion extraction. Ion density and electron temperature in the source are obtained with a Langmuir probe. The ion temperature was measured in a similarly produced and contained plasma with an electrostatic retarding field analyzer and is estimated to be given by the same value.[8] The ion source plasma parameters are summarized in Table I, as are the ion beam and the background plasma properties.

The ion source plasma chamber is insulated from, and contained within, a slightly larger chamber to separate it from the background plasma. The inner chamber is biased at a large positive potential, V_b, corresponding to the beam energy, with respect to ground to drive the ions through the extraction electrodes.

Several electrode structures were used depending upon beam requirements. A set of two planar stainless steel screens (4 lines/cm) produced a high beam current ($I_b \lesssim 0.5$ A), large diameter ($D \sim 19$ cm at source), but highly divergent beam (divergence half-angle $\theta \simeq 15°$). On the other hand, accel–decel electrodes, one at the inner chamber potential, one at the outer chamber potential, and a focusing electrode between the other two at a negative potential produced a low divergence ($\theta \simeq 1°$) ion beam. We will discuss only the accel–decel systems here.

Extraction Electrodes

One of the accel–decel geometries tested, a slit geometry, is shown in Fig. 3 along with beam profiles. The dimensions of the electrodes in the short direction are scaled up from the diameters of the electrodes used by Okamoto and Tamagawa.[9] In space charge limited flow, particle trajectories will be geometrically similar if all electrode dimensions are scaled proportional to the square root of the random ion current of the plasma in the source.[10] The ion beam current density was measured from the ion saturation current I_{is} of a small planar disk probe using the relation

$$I_{is} = n_b e \mathbf{v}_b \cdot \mathbf{A}_p, \tag{1}$$

where n_b is the ion beam density, $\mathbf{v}_b$ is the drift velocity of the beam, and A_p is the probe area. The ion saturation current due to any background plasma that might be present is much smaller than that given by Eq. (1) and is neglected. The slotted electrodes produced a beam well focused in the short direction of the slot but poorly focused in the long direction. The peaks at the edge of the beam in the long direction are due to end effects of the slit geometry. Since the peaks converge, a focused spot should occur at a sufficient distance from the source.

A single circular hole accel–decel electrode configuration with diameters equal to the slit heights, and interelectrode separations equal to those shown in Fig. 3 was also tested. The beam produced by these circular electrodes could be focused well in all lateral directions by adjusting the potential on the focusing electrode. Figure 4 (top) shows the ion beam current density profile for several values of the focusing electrode potential at constant beam energy illustrating the sensitivity of the focusing upon this potential. Similar beam profiles for fixed focusing electrode potential at several beam energies are plotted in Fig. 4 (bottom) showing that the optimum focusing electrode potential is a function of the ion beam energy. A change in the ion source density also affects the optimum focusing potential.

To provide a larger area beam, the multiple hole accel–decel electrode configuration shown in Fig. 5 was used. Each hole is identical to the single hole electrode described above. The ion beam current density profile, also shown in Fig. 5, is seen to exhibit a bumpy structure 15 cm away from the

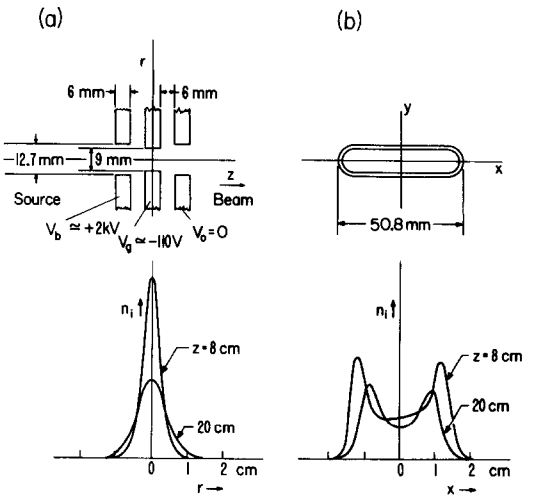

FIG. 3. (a) Single hole ion extraction system and typical radial beam profiles. (b) Geometry of the ion extraction system with slit geometry and ion beam profiles parallel to the slit. The narrow sides of the slit and the plate spacings are the same as in the single hole geometry.

TABLE I. Basic ion source and plasma data.

Gas, pressure		H_2, $p \lesssim 10^{-3}$ Torr
Ion source plasma	Power	$V_d = 36$ V, $I_d \leq 3$ A
	Density	$n_e \leq 5\times10^{10}$ cm^{-3}
	Temperature	$\kappa T_e \approx 0.6$ eV
		$\kappa T_i \approx 0.2$ eV
	Noise level	$\delta n_i/n_i \sim 0.1\%$ $(0 < f < 400$ kHz)
Ion beam	Energy	$0 < V_b < 5$ kV
	Velocity	$0 < V_b < 7\times10^7$ cm/sec (H_2^+)
	Current	$I_b = 10$ mA
	Current density	$J_b = 0.2$ mA/cm^2 ($V_b = 1$ kV)
	Beam density	$n_b = 0.5\times10^8$ cm^{-3}
		$\theta \approx 1°$ (half-angle at 50% density)
Background plasma	Density	$n_e \lesssim 10^9$ cm^{-3}
	Temperature	$\kappa T_e \simeq 0.6$ eV
	Magnetic field	$B_0 < 100$ G

source due to discrete holes and the low divergence of the beamlets. The beam appears to be a superposition of independent beamlets each having the properties described above. At sufficient distance the fine structure washes out.

rf MODULATION OF THE ION BEAM

It is found that a low level rf perturbation or a fast rise pulse on the ion beam propagates as a free-streaming ion disturbance along the beam direction. By free-streaming we mean that the dominant contribution to the *dispersion* of the disturbance (ω vs k) is due to the spatial bunching and debunching of noninteracting particles, and not by the zeroes of the plasma dispersion relation. These perturbations are analogous to those found in a klystron tube and the same description applies to both. We do observe, however, an *amplitude* dependence of the free-streaming perturbation upon background plasma caused by a change in dielectric constant near a normal mode of a longitudinal plasma oscillation. We describe below how one may use the measured free-streaming perturbation properties to diagnose the ion beam's drift velocity and ion species, and to give an approximate upper limit to the beam velocity spread v_t along the beam direction. Two methods are used, first, a pulse and time-of-flight technique, and second, a steady state rf modulation with an interferometer processing the detected perturbation.

Pulse and Time-of-Flight

The experimental arrangement is shown in Fig. 1. A short pulse (40 nsec, -50 V) is applied to the center grid of the beam modulation grid. The center grid is shielded on all sides by highly transparent grids in order to reduce direct pickup of the rf signal. The outer grids are negatively biased so as to prevent electrons from being perturbed. The structure is placed perpendicular to the beam a few centimeters from the source. A small magnetic field, $B_0 \lesssim 30$ G, is applied perpendicular to the beam direction to further prevent free-streaming electrons from contributing to the response, but still allowing the beam ions to traverse the field essentially undeflected. The axially movable gridded rf probe picks up the amplitude of the perturbation of the ion beam due to the applied pulse at various distances from the source. This signal is displayed on a sampling oscilloscope, which has been triggered by the applied pulse, and traced on an x–y recorder.[3] The pulse response occurs delayed in time corresponding to $t = x/v_b$. When multiple ion species are present there will be a corresponding number of pips in the detected response due to different speed. This is the case for H_2 gas, where H^+, H_2^+, and H_3^+ are seen simultaneously. A typical distance vs time plot is shown in Fig. 6. A response was seen for both the rising and falling edge of the applied pulse for

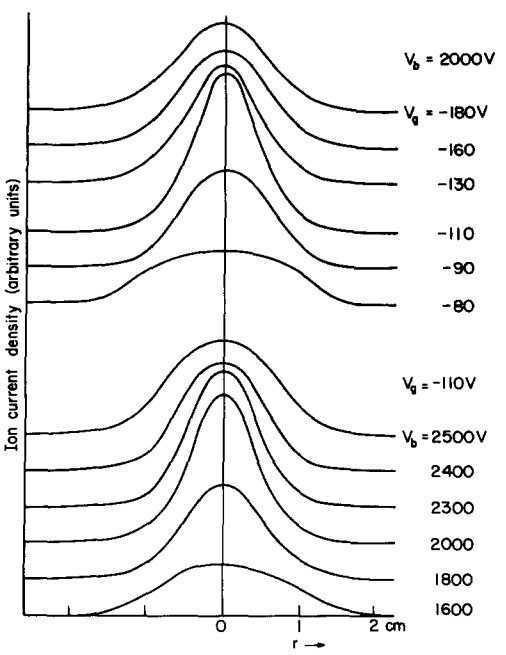

FIG. 4. Dependence of ion beam profile on grid and beam voltages. The traces are offset for purpose of display.

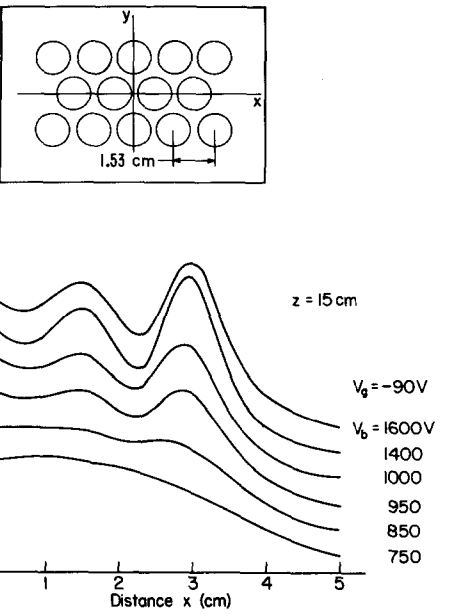

FIG. 5. Multihole multiaperture ion extraction system and beam profiles at different beam velocities. The traces are offset for purpose of display.

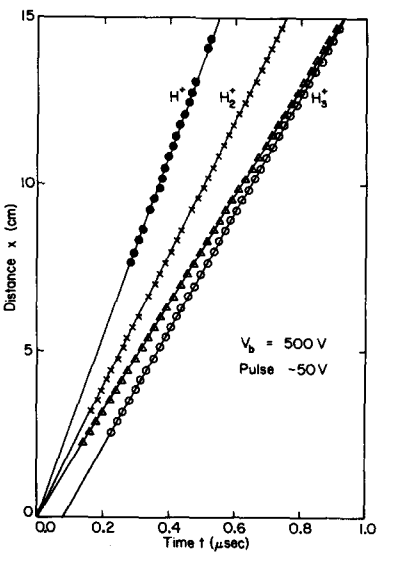

FIG. 6. Space–time diagram from time-of-flight measurements showing presence of different ion species. For H_3^+ the response due to pulse rise and fall are shown to indicate velocity modulation (0.9 μH_2; $V_b = 500$ V; applied pulse -50 V, 40 nsec).

each species with the difference in velocity corresponding to the effective potential on the modulating structure. From the observed bunching distance, $L\sim30$ cm, and pulse delay at $x=0$, $\Delta t\sim80$ nsec, we determine the effective velocity modulation to be $\Delta v_b/v_b=(v_b\Delta t/L)\approx8.8\times10^{-2}$ for an applied modulation voltage $\Delta V_b/V_b=0.1$. Note that the response due to the rising pulse edge yields the correct beam velocity, $v_b=1.78\times10^7$ cm/sec, for H_3^+ at $V_b=500$ V and that the measurement accuracy is excellent ($\sim1\%$).

Steady State rf Modulation

The same probe and grid arrangement used in the pulse and time-of-flight method is used for steady state rf modulation ($f_m\simeq100$ MHz, $V_m\lesssim15$ V rms) of the ion beam. The amplified signal from the movable rf probe, $V\propto\cos(\omega t-kz)$, and a reference signal from the oscillator, $V\propto\cos(\omega t)$, are mixed and time-averaged so as to display the spatial dependence, $\cos(kz)$, on an x–y recorder as a function of the pickup probe position. For free-streaming disturbances, the wavelength λ and frequency f are related to the beam drift velocity v_b by

$$\lambda f=v_b \tag{2}$$

when the beam velocity spread v_t is much smaller than v_b. The beam velocity, in turn, is related to the beam potential V_b by

$$\tfrac{1}{2}Mv_b^2=eV_b, \tag{3}$$

where M is the ion mass.

Several characteristic interferometer traces are shown in Fig. 7 for the following cases of ion species: (a) H_2^+; (b) a mixture of H_2^+ and H_3^+; (c) He^+; and (d) Ar^+. The case of a mixture of species [Fig. 7(b)] is particularly interesting since a spatial beating occurs due to the superposition of two signals with different wavelengths. The depth of the beats is an indication of the relative abundance of the two species and in the case of Fig. 7(b) indicates amost equal amounts of H_2^+ and H_3^+. The presence of H^+ was not detected by this method due to the relatively small concentration.

The measured phase velocity, λf, which by Eq. (2) is

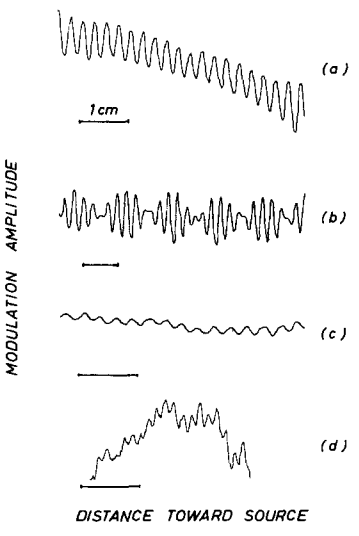

FIG. 7. Interferometer traces of modulated ion beams of different species (a) H_2^+ (0.7 μ, 1.6 kV, 130 MHz); (b) H_2^+ and H_3^+ (1 μ, 1.5 kV, 130 MHz); (c) He^+ (1 μ, 2 kV, 109 MHz); (d) Ar^+ (1 μ, 5 kV, 109 MHz).

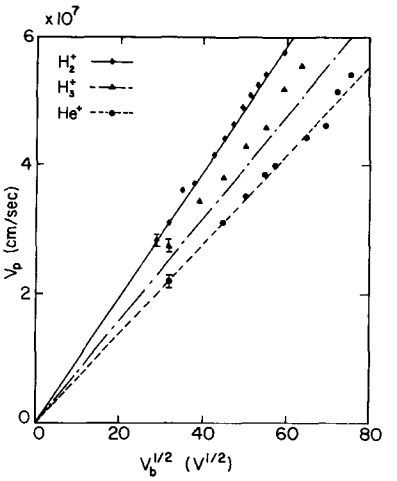

FIG. 8. Phase velocity $v_p=\lambda f$ of beam modulation versus beam voltage $V_b^{\frac{1}{2}}$ for different ion species. Dashed lines are theoretical curves for H_2^+, H_3^+, and He^+ ions. ◇—0.7 μ H_2, $f=109$ MHz, discharge 43 V, 0.5 A; △—1.0 μ H_2, 50 V, 1 A; ○—1 μ He, 109 MHz, 52 V, 0.25 A).

equal to the beam drift velocity, is plotted in Fig. 8 as a function of the square root of the beam voltage for three different situations. When the hydrogen gas pressure is adjusted to give a predominantly H_2^+ beam the phase velocity agrees with the H_2^+ velocity given by Eq. (3). A He^+ beam also agrees well with theory. When there is a mixture of H_2^+ and H_3^+ present in the beam the phase velocity lies between the values expected for H_2^+ and H_3^+ above. This is because a spatial beat between a wave with wave number k_1 and another with wave number k_2 has a wave number given by $k=(k_1+k_2)/2$ and hence a phase velocity between that of H_2^+ and H_3^+. The number of wavelengths between two nodes of a beam is $L=(k_1+k_2)/[2(k_1-k_2)]=(\sqrt{m_1}+\sqrt{m_2})/[2(\sqrt{m_1}-\sqrt{m_2})]$. For H_2^+ and H_3^+, $L=4.95\lambda$ which is demonstrated in Fig. 7(b) along with the characteristic phase jump of π radians at the nodes.

The ion velocity spread v_t on a given beam may be obtained by observing that the damping of the free-streaming perturbation due to phase mixing goes approximately as $e^{-\gamma z}$ where $\gamma=(v_t/v_b)k$ when $v_t\ll v_b$. A limit of $v_t/v_b<0.005$ may be obtained by observing an amplitude e-folding length $z\approx30\lambda$. This is only an estimate of the upper limit on v_t/v_b since neither the exact modulation mechanism nor additional collisional damping is known.

ENHANCEMENT OF rf PERTURBATIONS

It was experimentally found that when the ion beam traverses a denser background plasma perpendicular to the magnetic field the amplitude of the free-streaming perturbations is a maximum when the frequency is between electron cyclotron harmonics. This effect is demonstrated in Fig. 9. The background plasma density to beam density is large enough to avoid the electron cyclotron drift instability and the perturbations follow the beam dispersion (forward wave) and not the Bernstein wave dispersion (backward wave). It is believed that the amplitude enhancement of the free-streaming perturbations is a passive dielectric response of the plasma to the electric field of the bunching and debunching ions in the beam. As the free-streaming dispersion (ω,k) approaches a plasma resonance (Bernstein wave dispersion) the plasma dielectric decreases and hence the

amplitude increases. The free-streaming wave dispersion depends only upon the ion beam distribution function, however, as in the case of ballistic electron plasma wave echoes.[11]

ION BEAM-PLASMA INSTABILITIES

Two ion beam–plasma instabilities have been identified so far when the ion beam traverses a background plasma perpendicular to the magnetic field, i.e., the electron cyclotron drift instability and an instability at the lower hybrid frequency. Figure 10 shows the enhanced plasma noise spectra at both low frequencies ($f<2$ MHz) and high frequencies ($f\gtrsim f_{ce}$) due to these instabilities. The low frequency spectrum shows ion acoustic noise and, for certain ion beam parameters, a sharply enhanced noise peak at the lower hybrid frequency. The frequency of this peak agrees well with the lower hybrid frequency ω_{lh} calculated from

$$\frac{1}{\omega_{lh}^2}=\frac{1}{\omega_{ci}^2+\omega_{pi}^2}+\frac{1}{\omega_{ce}\omega_{ci}}, \tag{4}$$

where ω_{pi} is the ion plasma frequency, and ω_{ce} and ω_{ci} are the electron and ion cyclotron frequencies, respectively. The lower hybrid peak tracks properly with plasma density and magnetic field. A more detailed description of this instability will be published elsewhere.

For certain parameter regimes enhanced noise also appears in the electron cyclotron harmonic passbands due to the ion beam interacting unstably with the electron Bernstein waves as shown in Fig. 10(b). This noise also scales consistently with magnetic field and ion beam velocity and has been described in detail in Ref. 3.

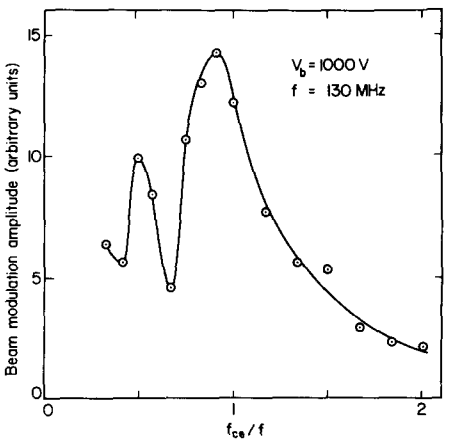

FIG. 9. Variation of beam modulation amplitude with magnetic field in the presence of a background plasma ($V_b=1000$ V; $f=130$ MHz; $n_e=4.7\times10^8$ cm^{-3}; $kT_e=0.6$ eV).

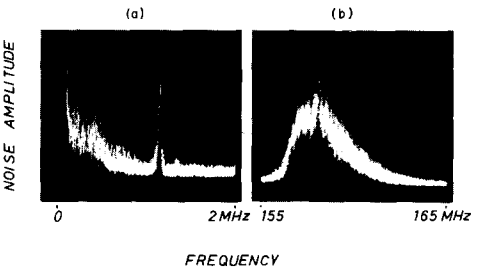

FIG. 10. Enhanced noise on ion beam in presence of magnetized background plasma. (a) Ion acoustic and lower hybrid frequency noise. (b) High frequency noise due to electron cyclotron drift instability.

ACKNOWLEDGMENTS

The authors thank K. R. MacKenzie for the use of his large volume plasma device and many useful comments, A. Y. Wong for his interest in the work, W. S. Cooper III for a useful discussion about ion source extraction, and Z. Lucky for his expert technical support. This work was supported by the Air Force Office of Scientific Research Contract # 72-2332.

[1]H. V. Wong, Phys. Fluids **13,** 757 (1970). S. P. Gary and J. J. Sanderson, J. Plasma Phys. **4,** 739 (1970). S. P. Gary, J. Plasma Phys. **4,** 753 (1970) and J. Plasma Phys. **6,** 561 (1971). C. N. Lashmore-Davies, J. Phys. A **3,** L40 (1970). A. Hirose and I. Alexeff, Nucl. Fusion **12,** 315 (1972). A. B. Mikhailovskii and E. A. Pashitskii, Zh. Tekh. Fiz. **35,** 1960 (1965) [Sov. Phys.-Tech. Phys. **10,** 1507 (1966)]. N. A. Krall and P. C. Liewer, Phys. Rev. A **4,** 2094 (1971).

[2]D. W. Forslund, R. L. Morse, and C. W. Nielson, Phys. Rev. Lett. **25,** 1266 (1970) and Phys. Rev. Lett. **27,** 1424 (1971); D. Forslund, R. Morse, C. Nielson, and J. Fu, Phys. Fluids **15,** 1303 (1972). M. Lampe, W. M. Manheimer, J. B. McBride, J. H. Orens, R. Shanny and R. N. Sudan, Phys. Rev. Lett. **26,** 1221 (1971). M. Lampe, W. M. Manheimer, J. B. McBride, J. H. Orens, K. Papadopoulas, R. Shanny, and R. N. Sudan, Phys. Fluids **15,** 662 (1972). K. Papadopoulos, R. C. Davidson, J. M. Dawson, I. Haber, D. A. Hammer, N. A. Krall, and R. Shanny, Phys. Fluids **14,** 849 (1971).

[3]B. H. Ripin and R. L. Stenzel, Phys. Rev. Lett. **30,** 45 (1973).

[4]M. Keilhacker and K. H. Steuer, Phys. Rev. Lett. **26,** 694 (1971).

[5]R. L. Stenzel, Phys. Fluids , **April (1973) (to be published).**

[6]H. Ikezi and R. J. Taylor, Phys. Rev. Lett. **22,** 923 (1969).

[7]R. Limpaecher and K. R. MacKenzie, Bull. Am. Phys. Soc. **16,** 1222 (1971).

[8]H. Ikezi and R. J. Taylor, J. Appl. Phys. **41,** 738 (1970).

[9]Y. Okamoto and H. Tamagawa, Rev. Sci. Instrum. **43,** 1193 (1972). W. S. Cooper, K. H. Berkner, and R. V. Pyle, Nucl. Phys. **12,** 263 (1972).

[10]P. Kirstein, G. Kino, and W. Waters, *Space Charge Flow* (McGraw-Hill, New York, 1967).

[11]B. H. Ripin and R. E. Pechacek, Phys. Rev. Lett. **24,** 1330 (1970) and Phys. Fluids **15,** 1980 (1972).